Phys. Status Solidi A **214,** No. 10, 1700295 (2017) / **DOI** 10.1002/pssa.201700295

physica status solidi a
www.pss-a.com
applications and materials science

Self-assembled dielectric microsphere as light concentrators for ultrathin-silicon-based photodetectors with broadband enhancement

Gongjin Li[†,1], Qinglei Guo[†,1], Yangfu Fang[1], Shiwei Tang[1], Minjie Liu[1], Gaoshan Huang[1,2], and Yongfeng Mei[*,1]

[1] Department of Materials Science, Fudan University, Shanghai 200433, P. R. China
[2] State Key Lab of Silicon Materials, Zhejiang University, Hangzhou 310027, P. R. China

Received 11 May 2017, revised 1 June 2017, accepted 23 June 2017
Published online 20 July 2017

Keywords dielectric microsphere, light trapping, photodetector, ultrathin-silicon

[*] Corresponding author: email yfm@fudan.edu.cn, Phone: +86 21 656 43615, Fax: +86 21 556 65503
[†] These authors contributed equally to this work.

Owning to their superior electronic and optical properties, silicon nanomembranes (NMs) have attracted considerable attention to be exploited as fundamental building blocks for the applications in electronics, photonics, and optoelectronics. Nevertheless, small photon traveling distance in such ultra-thin silicon (UT-Si) nanomembranes with nanoscale thicknesses (50 nm) induces low total light absorption, which is crucial for optoelectronic applications. Here, a convenient and controllable strategy, involving self-assembly of dielectric polystyrene (PS) microsphere array on UT-Si, was proposed to enhance optoelectronic responses of UT-Si-based photodetectors in broadband. Scattering effect of PS microspheres facilitates to couple incident light into UT-Si layer, thus enhancing the light absorption. UT-Si-based metal-semiconductor-metal (MSM) photodetectors with a PS microspehere array demonstrate significant enhancement in optoelectronic response compared with the photodetector without PS microspeheres. Furthermore, the response spectrum can be controllably tuned by adjusting the size of paved microspeheres. This research may provide a practical and cost-efficient approach for enhancing the optoelectronic responses of nanomaterials with nanoscale thicknesses, thus expediting their potential applications in optoelectronic devices.

1 Introduction Single-crystalline silicon nanomembranes (NMs) [1–4] have been widely explored for applications in optoelectronic devices, such as lasers [5, 6], light emitting diode [7], solar cells [8], modulators [9], phototransistors [10], and photodetectors [11, 12], owing to their unique electrical and optical properties [1, 2]. Yet, such benefits are balanced by the insufficient light absorption in the nanoscale thickness of SiNM due to the small photon traveling distance [13–15], thus leading to a much lower photoelectric conversion efficiency in optoelectronic devices [16]. Most of present methods for enhancing light absorption in Si involve patterning macroscopic textures on the top surface, which redirects the light propagation to increase the light path in the active layer [17–21]. However, these macroscopic structure patterning approaches are not suitable for ultrathin-silicon (UT-Si) -based devices, such as SiNM, where the thickness may be less than a few hundred nanometers [22]. To improve the light absorption in ultrathin membranes, various light trapping strategies have been explored, such as reducing the reflection and/or concentrating light field by nano-structured Si (e.g., nanocone arrays [16], and photonic crystals [23]), extending the optical path by back reflectors or wrinkled surfaces [10, 24], coupling the incident light through surface plasmon resonance or plasmonic scattering (metal or dielectric nanostructures, e.g., nanoparticles [14, 15, 25, 26], nanogrooves [27]). Among these strategies, utilizing micro/nano-structured dielectric medium layer has been demonstrated to be a particularly promising approach because of their outstanding optical benefits without bringing any

undesirable degradation of electrical performance, as well as its simple and convenient process [25, 28–30].

Here, a convenient and controllable strategy is proposed to integrate polymer-based microspheres with single-crystalline UT-Si to yield metal-semiconductor-metal (MSM) photodetectors with enhanced optoelectronic response by scattering induced light trapping effect. Physical mechanisms of enhanced light absorption in UT-Si induced by the PS microsphere layer are discussed in detail. A broadband with more than 180% enhancement in optoelectronic response (e.g., photocurrent) is achieved experimentally compared with that of bare UT-Si-based device. Furthermore, by changing the size of coupled microspheres, the photocurrent spectrums (PCSs) of UT-Si-based photodetectors can be well-tuned, which agrees well with the prediction of theoretical simulations. This research may provide a simple and realizable approach to improve the performance of ultrathin semiconductor membrane-based photodetectors, thus expediting its potential applications in optoelectronics.

2 Experimental

2.1 Photodetector fabrication The thickness of lightly boron-doped UT-Si and buried oxide layer are 50 and 120 nm, respectively. After removing the natural oxide layer of UT-Si by immersing the SOI slice into 1% HF solution, patterned Ti/Au (20/50 nm) electrodes were deposited by electron beam evaporation. The channel length and width were defined as 200 and 1000 μm through a shadow mask. Then source and drain contacts were activated by rapid thermal annealing in N_2 at 450 °C for 3 min, and the device was encapsulated into a DIP chip holder (NTK, Inc.) by wire bonding process (WEST BOND 7476D). The PS microspheres were bought from Janus New Materials Co., Ltd., which were synthesized by emulsion polymerization, and the PS microsphere emulsion was prepared by mixing PS microspheres with ethyl alcohol and deionized water. Then, PS microsphere arrays on UT-Si were formed by utilizing gravity sedimentation method [32]. To achieve a PS microsphere array with high-quality arrangement, the suspension concentration of PS microspheres is critical. Here, PS emulsion was diluted in ethyl alcohol and deionized water mixture with a mass ratio of 3:10:6. Then, the suspension was drop-casted on the UT-Si surface that the layer number can be well controlled by the suspension amount. Notably, the UT-Si surface should be hydrophilic to ensure a good spread capability of PS microspheres. In this case, the surface modification of UT-Si was realized by immersing them into Piranha solution for 30 s, and the followed soaking in the mixing solution of ammonium hydroxide and hydrogen peroxide (H_2O:$NH_3 \cdot H_2O$:H_2O_2 = 5:1:1) for 30 min.

2.2 Measurements To analyze the performances of UT-Si-based photodetectors, measurements were carried out with the same device before and after paving the PS microspheres. The current–voltage characteristics of photodetectors in dark and illumination conditions were obtained by semiconductor parameter analyzer (Kiethley 4200-SCS/F), and light source was supplied by a white fluorescent lamp (HX LAMP, 8 W in power). The transient response properties and photocurrent spectroscopy were attained by electrochemical workstation (Zahner PP211 IM6), and the light sources were supplied by CIMPS TLS02 light and TLS03 tunable light, respectively.

3 Results and discussion

3.1 Broadband enhancement in light absorption of UT-Si For free-standing UT-Si, the total light absorption may compromise compared with the bulk one, due to the small photon traveling distance [13–15]. However, the average absorption per unit thickness for UT-Si is calculated to be far larger than that of bulk Si (more details can be found in Fig. S1 and Supporting Information), thus providing promising potentials for the application in ultra-sensitive detecting devices. Furthermore, when integrating the UT-Si on a SiO_2/Si substrate, i.e., silicon-on-insulator (SOI) materials shown in Fig. 1a (transmission electron microscope image), light absorption in UT-Si could be further enhanced compared with that in a free-standing one, especially in short-wavelength band (about 480–600 nm) as calculated in Fig. 1b and Fig. S2. Finite difference frequency domain (FDFD) algorithm is utilized to analyze the field intensity distribution in the stacked multilayers under light illumination, and the incident light wavelength is set as 480 nm. More details about FDFD simulation can be found in supporting information. Figure 1b shows the electric field intensities distributed in different stacked layers with obvious variations along the depth (z direction) but uniformly distributed along x direction, which can be attributed to interference interactions in this multilayer structure. Besides, the maximum value of the electric field intensity exactly occurs in the UT-Si layer, which would lead to enhanced light absorption and improved performances in UT-Si-based optoelectronic devices. High-resolution transmission electron microscope (HRTEM) is performed to verify the single-crystalline characteristic of the UT-Si utilized in this work, as displayed in the inset of Fig. 1c, which sketches the structure of UT-Si on SiO_2/Si.

Broadband enhancement in light absorption of UT-Si can be further achieved by paving dielectric microspheres as light concentrators onto UT-Si on insulator, as schematically shown in Fig. 1d. Hexagonal close-packed polystyrene (PS) microspheres with microscale diameter and negligible parasitic absorption [31] on the top surface of UT-Si are obtained by gravity sedimentation process with a carefully hydrophilic treatment of the substrate [32], as demonstrated in Fig. 1e. When illuminated by a light source, dielectric PS microspheres layer will serve as another medium to couple light into the UT-Si layer [33]. The whole construction can be modeled as stacked multi-layers (i.e., Si Sub., SiO_2, UT-Si, PS microsphere layer, and air from bottom to top), as shown in the inset of Fig. 1f. Corresponding refractive indices are calculated and plotted in Fig. 1f. When light

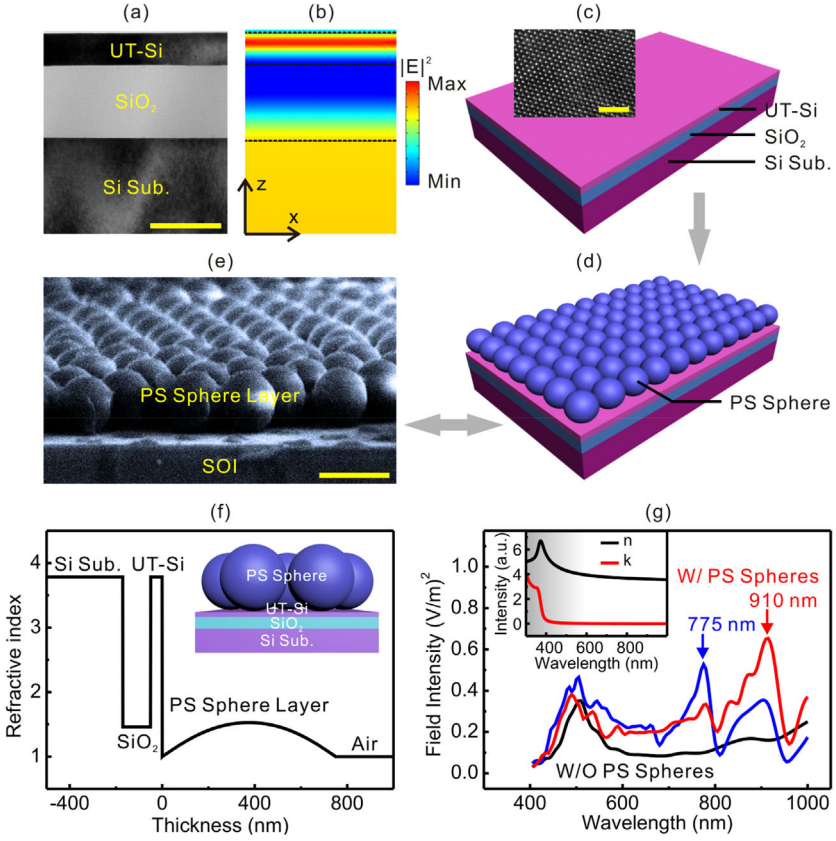

Figure 1 (a) Cross-section view of UT-Si on insulator obtained by TEM. The scale bar is 100 nm. (b) Electric field intensity distribution in the (x, z)-plane of UT-Si on insulator under light illumination with the wavelength of 480 nm. (c) Schematic of UT-Si on insulator. Inset displays HRTEM image of UT-Si. The scale bar is 5 Å. (d) Schematic of paved PS microsphere layer/UT-Si on insulator construction. (e) Tilted view of hexagonal close-packed PS microsphere arrays obtained by SEM. Scale bar is 1 μm. (f) The effective refractive index profiles of the stacked multilayers. Inset displays schematic illustration of 50 nm thick UT-Si paved with PS microsphere layer. (g) Calculated average field intensities in UT-Si layer: with PS microspheres (blue line: 750 nm in diameter; red line: 900 nm in diameter.) and without PS microspheres (black line). Inset displays the dispersion of refractive index and extinction coefficient of silicon.

passes through different media, the reflectance can be described by the Fresnel equation, $R = [(n_1 - n_2)/(n_1 + n_2)]^2$, where n_1 and n_2 are refractive indices of two contiguous media. Smaller difference between n_1 and n_2 apparently represents lower reflectance of the incident light. As demonstrated in Fig. 1f, the effective reflection index of the paved PS microsphere layer locates between air and UT-Si, therefore, the reflectance of UT-Si on insulator after paving the PS microspheres would be suppressed. In addition, because the sizes of the paved PS microspheres (several hundred nanometers) are comparable with the wavelengths of incident light source, they could also diffractively couple and trap the incident light into the underneath UT-Si layer [28], thus enhancing the light absorption. According to the above analysis, electric field intensities in UT-Si with PS microspheres are calculated by FDFD algorithm, and the case for pure UT-Si is also calculated for compassion. Two types of PS microspheres with diameters of 750 and 900 nm are involved. All the calculated results are summarized in Fig. 1g marked as "W/ PS Spheres" for UT-Si with PS microspheres (blue line: 750 nm in diameter; red line: 900 nm in diameter) and "W/O PS Spheres" for pure UT-Si (black line), respectively. The dispersion of refractive index and extinction coefficient of silicon utilized in the simulation are shown in the inset. After paving the PS microsphere layer, both cases exhibit enhanced field intensity in a wide spectrum range (especially at long wavelength band, 600–1000 nm). Notably, remarkable enhancements occurring at 775 and 910 nm (marked with arrows in Fig. 1g) are observed for the cases of UT-Si paved with 750 and 900 nm PS microspheres, which will be discussed later.

In brief, at short-wavelength band (400–600 nm), interference interactions play a dominant role that light absorption in UT-Si can be significantly enhanced by integrating it with SiO_2/Si substrate. For long-wavelength band (600–1000 nm), enhanced light absorption can be achieved by paving PS microspheres, which act as either textured antireflection or light trapping coating, thus allowing more light to be absorbed by the underneath UT-Si layer. Notably, the light absorptions in UT-Si are strongly dependent on the sizes of paved PS microspheres and wavelengths of the incident light (Fig. 1g).

3.2 Physical mechanisms of enhanced light absorption in UT-Si In order to further understand the underlying physical mechanism, both size and wavelength effects on the electric field intensity distribution of the PS microsphere/UT-Si on insulator system are taken into consideration. For simplicity, four representative cases with two PS microsphere diameters (D, 600 and 900 nm) and two light wavelengths (λ, 600 and 900 nm) are simulated, and the electric field intensity distributions for each case are illustrated in Fig. 2. Normally incident lights are obviously

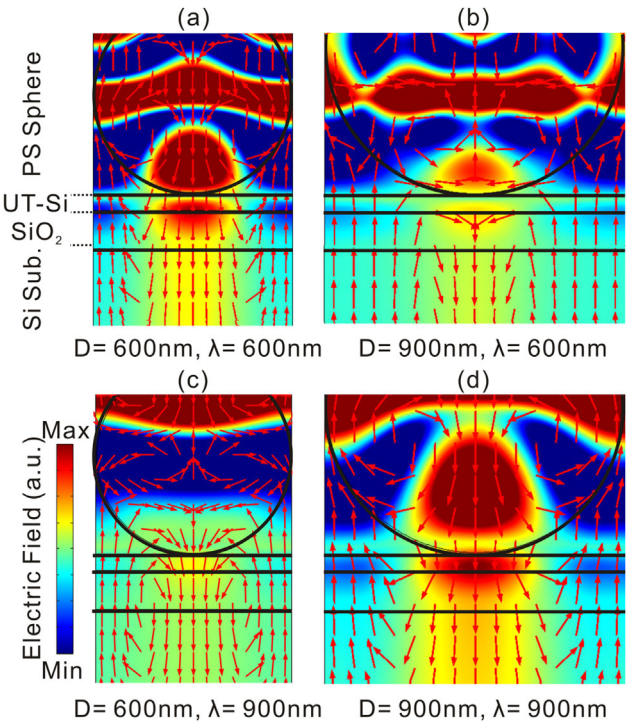

Figure 2 (a–d) Cross section views of normalized electric field intensity and energy flux distribution in PS Sphere/UT-Si/SiO_2/Si substrate constructions with different PS microsphere diameters and illuminated light wavelengths. Diameters of microspheres and wavelengths of irradiated light are labeled at the bottom.

scattered with altered propagation direction by paved PS microspheres, which could act as light coupling concentrators [34, 35]. Therefore, the light paths in UT-Si would be distinctly enhanced, and the probability of photo-generation per incident photon would be increase [36]. It has been previously demonstrated that the scattering behavior is strongly dependent on the size of silicon spherical nanoparticles [37]. For PS microspheres in our present work, similar size-dependent scattering effect can also be observed. When the diameter of PS microsphere is almost equal with the irradiated light wavelength, the scattering effect becomes much stronger that large amount of the incident light are firstly trapped into the underneath UT-Si layers. The powerful scattering could cause transverse waveguide mode [38], which couples and guides the light into the almost whole UT-Si, as illustrated in Fig. 2a and d. For the cases that the irradiation wavelength has large deviation with the microsphere diameter, however, the scattering behavior is relatively weak, as shown in Fig. 2b and c. Nevertheless, the paved PS microspheres still serve as the antireflection coating layer, which determined by the effective reflection index of PS microsphere layer as discussed in Fig. 1f.

As a result, for the PS microsphere layer with a constant diameter, light trapping effect induced by scattering will play a dominant role when the wavelength of incident light is equal/comparable to the diameter. As for the other wavelengths, though the light trapping effect is relatively weak, antireflection effect can still contribute to the enhancement of the light absorption by reducing the light reflection. A good understanding of the physical mechanisms of the light absorption enhancements in UT-Si by PS microspheres would guide us to improve the optoelectronic response of UT-Si-based photodetectors, and to artificially tune the response wavelength by adjusting the size of PS microspheres.

3.3 Enhanced optoelectronic response in UT-Si-based photodetectors The UT-Si on insulator with paved PS microspheres was further constructed into a MSM type photodetector. Thicknesses of the top UT-Si and SiO_2 layer are 50 and 120 nm, respectively. The fabrication process begins with constructing photodetectors with UT-Si on insulator. After the optoelectronic response properties were measured, a monolayer of PS microspheres was paved on UT-Si of the same device by self-assembly. Plane view of a typical device obtained by SEM is illustrated in Fig. 3a,

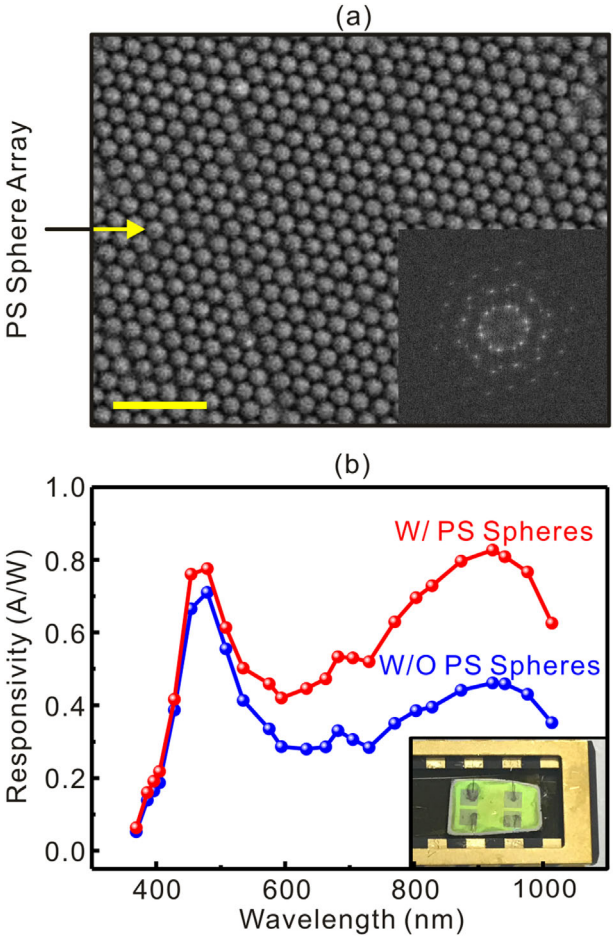

Figure 3 (a) SEM image of hexagonal close-packed PS microsphere array. Scale bar is 5 μm. Inset shows the corresponding Fourier transform. (b) PCSs of UT-Si-based photodetectors with (W/) and without (W/O) PS spheres. Inset shows the digital photograph of UT-Si photodetector encapsulated on a DIP chip holder.

where a monolayer of PS microspheres uniformly covers on UT-Si. Corresponding Fourier transform image with typical hexagonal pattern is displayed in the inset, which indicates that the PS microspheres self-assemble into hexagonal close-packed colloidal crystal structure. Large area of PS microsphere array stacking on the UT-Si is further demonstrated in Fig. S3a. To confirm the device stability during optoelectronic characterization, all devices were encapsulated into ceramic dual-in-line package (DIP) chip holders. Detail of the photodetector on DIP is displayed in the inset of Fig. 3b.

For the UT-Si-based MSM photodetectors with two back-to-back Schottky contacts, the barrier heights for holes and electrons are calculated to be 0.84 and 0.86 eV, respectively. Calculation details and energy-band diagram between UT-Si and two titanium electrodes can be found in Supplementary Information and Fig. S4. In the dark, the current is limited by the low injection of carriers at the contacts, which facilitates to reduce excess noise in the optoelectronic receiver [39, 40]. When irradiated, additional carriers are generated and separated by the external electric field, thus induces a large photocurrent. Since the PS microspheres paving process has negligible influence on the contact properties of photodetectors, the Schottky barriers with/without microspheres are considered as same. The relative simple device structure of MSM photodetector leads to a reliable optoelectronic performance, making it easy to distinguish the enhancement from PS microsphere arrays.

We should stress that testing the same device before and after PS microspheres paved can avoid any complications due to the inhomogeneity of different devices. Figure 3b shows the typical photocurrent spectrums (PCS) of UT-Si-based photodetectors with and without PS microspheres. After paving the PS microspheres, the responsivity of UT-Si-based photodetector exhibits broadband enhancement (600–1000 nm) in responsivity compared with that of the device without PS microspheres. The diameter of the paved PS microspheres here is 750 nm, therefore, the responsivity should reach maximum value at equal/comparable wavelength, e.g., 775 nm, based on the above discussions in Sections 2.1–2.2. However, after paved with PS microspheres, the UT-Si based photodetector exhibits broadband enhancement (from 600 to 1000 nm) in photocurrent, as shown in Fig. 3b. This paradox between the experimental and theoretical results can be eliminated if the size-distribution of the paved PS microspheres is taken into consideration, which will be discussed later.

Since the paved PS microsphere diameter and irradiation wavelength could strongly influence the light absorption in the UT-Si, the enhancements of electric field intensities under different sizes and wavelengths are further calculated by utilizing FDFD algorithm with tabulated material optical constants [41, 42]. Two-dimensional topography of the enhancements varying with the diameters of the PS microspheres and the irradiation wavelength is illustrated in Fig. 4a. The color bar refers to the enhance factor ($|E|^2/|E_0|^2$), where E_0 and E denote the average electric

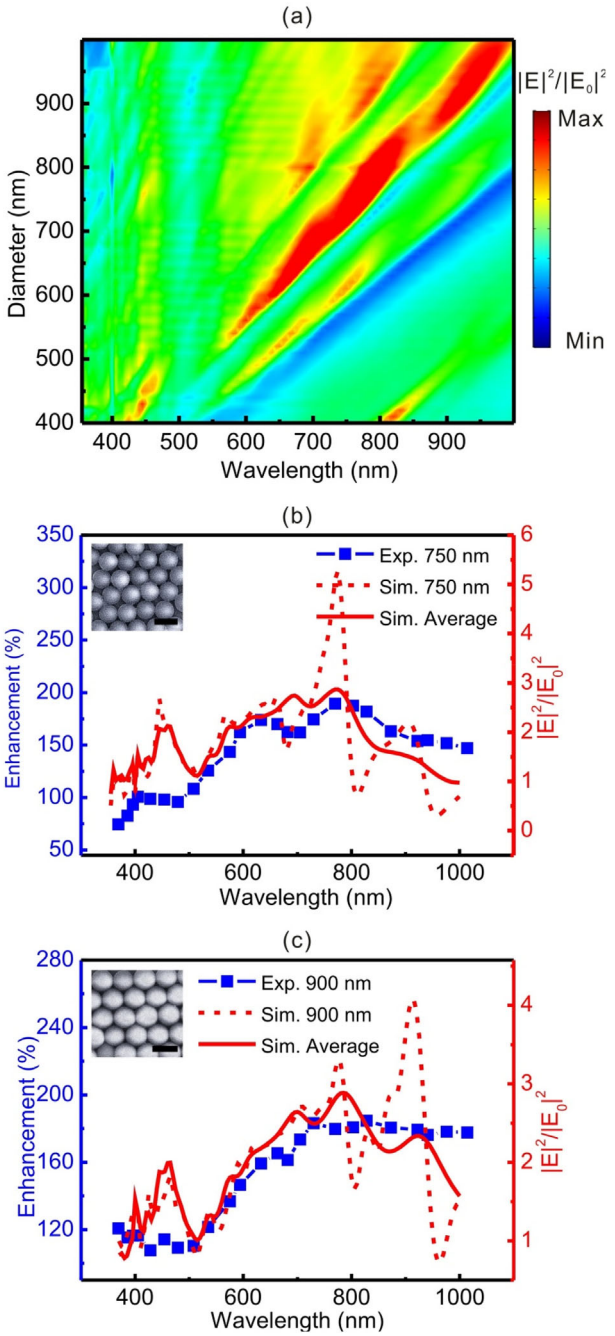

Figure 4 (a) Two dimensional topography of the electric field intensity ratio ($|E|^2/|E_0|^2$) as functions of light wavelengths and the diameters of microspheres. (b and c) Experimental photocurrent enhancements (blue dotted line), simulated electric field intensity enhance ratios with a certain diameter (red dotted line), and simulated electric field intensity enhance ratios weighted by size distribution (red line) of UT-Si with the paved PS microspheres diameter of 750 nm (b), 900 nm (c). The insets display the corresponding SEM image of PS microspheres. All scale bars are 1 μm.

filed intensities in UT-Si before and after paving PS microspheres, respectively. In the spectrum range of 400–600 nm, the enhancement is not so sensitive to the irradiation wavelength and microsphere diameter. As analyzed in Section 3.1, strong interference effect from the SOI structure in this spectrum region significantly enhances the electric field intensity, thus the enhancement induced by paving dielectric microspheres is not so distinct. In the range from 600 to 1000 nm, however, the field enhancement becomes sensitive to the irradiation wavelength and reaches the maximum value when the wavelength of incident light is approximately equal with the size of PS microspheres. This two-dimensional topography of resonant enhancement can serve as the guidance to tune the optoelectronic response enhancement of UT-Si-based photodetectors by adjusting the size and/or size-distribution of the paved PS microsphere layer.

With the aim of demonstrating the above conclusion, PS microspheres with median diameters of 750 and 900 nm were employed to pave on the surface of UT-Si-based photodetectors, and the corresponding photocurrent spectrum (PCS) was characterized at a bias of 3 V. Distinct enhancements, which are defined as the ratio of photocurrents after and before paving the PS microspheres, are obtained at the wide range from 400 to 1000 nm, as summarized in Fig. 4b and c (blue squares). Simulated result by utilizing PS microspheres with a constant diameter (i.e., 750 or 900 nm) is extracted from Fig. 4a to fit the experimental result. For the case that the diameter of PS microsphere is 750 nm, enhancement reaches the maximum value at 775 nm, nevertheless accompanied by distinct deviations compared with the experimental results, as shown in Fig. 4b (red dotted line). The simulation result could be optimized by weighting the enhancements shown in Fig. 4a according to practical size distribution of the paved PS microspheres (mean diameter: 750 nm, distribution: 20%; see Fig. S3b, Supplementary Information), and the deviations are significantly reduced as demonstrated in Fig. 4b (red solid line). Similar results can be observed when PS microspheres with a median diameter of 900 nm were utilized, as illustrated in Fig. 4c. We believe that the optoelectronic response of UT-Si-based photodetectors can be further tuned and artificially controlled by adjusting the size distribution of PS dielectric microspheres paved on the surface of UT-Si.

Apart from the photocurrent enhancement which is crucial for the responsivity of a light detection device, the parameter of response rate also plays an important role to evaluate the performance of a photodetector. With the aim of practical applications, the response rate of UT-Si-based photodetector should not degrade after paving the light trapping coating, i.e., PS microsphere array. In order to estimate the influence of PS microspheres on the response rate to the illuminated light, transient response properties of photodetectors with/without PS microspheres under switched blue light illumination at a bias of 10 V are characterized. Figure 5a shows the time-dependent power density of the switched LED with the wavelength of about 470 nm (orange dots) and photocurrents of both photodetectors, respectively. The switch-on time of light source is less than 10 μs. For the photodetector with PS microspheres

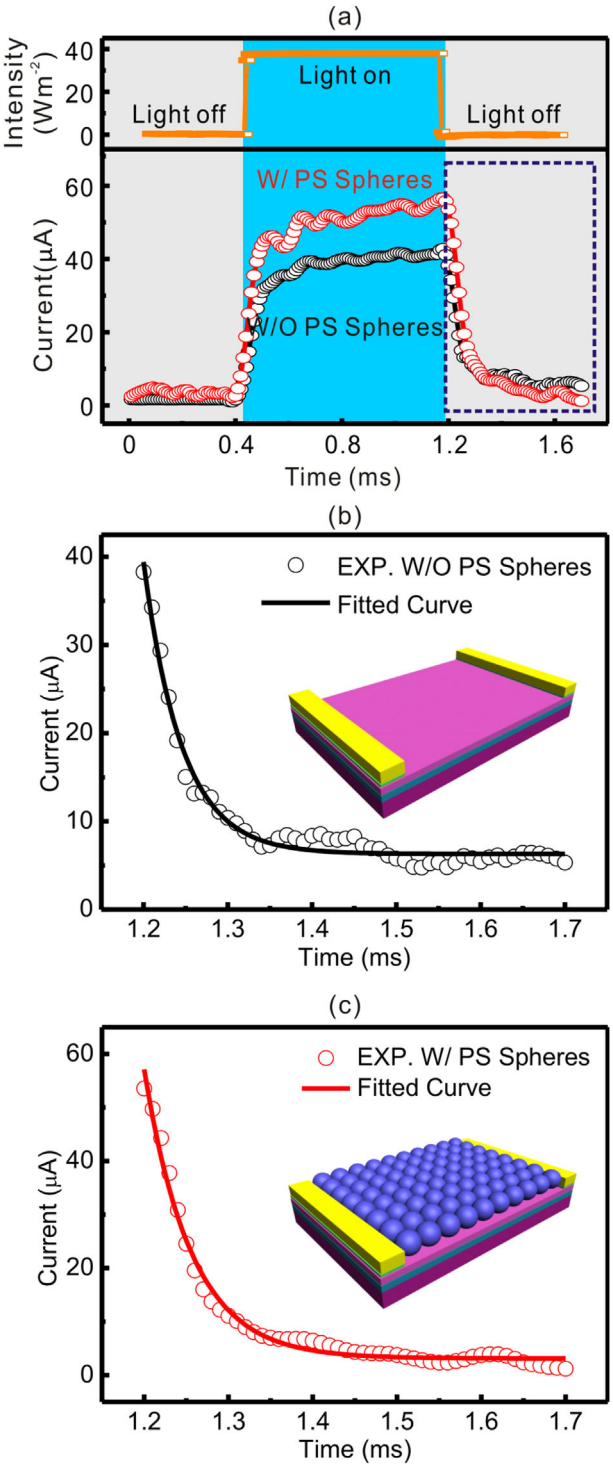

Figure 5 (a) Transient response of UT-Si based photodetectors without/with PS Spheres. (b and c) Magnified fall edges of both two devices (with and without PS Spheres).

(marked with "W/PS Spheres"), the corresponding photocurrent takes about 80 μs to rise to the 90% of a quasi-stationary state (about 50 μA), which is comparable with the device without PS microspheres (~70 μs, marked with "W/O PS Spheres"). When switching off the illuminated light, photocurrents of both photodetectors with/without PS microspheres decay rapidly. The photocurrent decay edges of both two types of photodetectors are magnified in Fig. 5b and c, respectively. Fitting decay edges with a single exponential decay mode [43], the values of fall times (τ) for UT-Si-based photodetectors with/without PS microspheres are obtained as 56 and 45 μs, respectively. The comparable rise/fall times between two types of UT-Si-based photodetectors (with and without PS microspheres) indicates that no compromise in response rates is created in UT-Si-based photodetectors when paved with PS microspheres.

4 Conclusions In conclusion, single-crystalline ultrathin-silicon (UT-Si) on insulator are demonstrated with enhanced light absorption compared with free-standing UT-Si due to a strong interference effect induced by the stacked multilayers. The optoelectronic response of UT-Si-based photodetectors can be further improved by paving the dielectric microspheres on them. Experimental and theoretical results indicate that the paved PS microsphere layer can serve as scattering and antireflection coatings to trap more light into the underneath UT-Si, and enhance the light absorption, thus improving the optoelectronic response in UT-Si-based photodetector. Additionally, tunable optoelectronic response could be achieved by controlling the size and/or size-distribution of dielectric microspheres. This study may provide a steerable and easily achievable strategy for improving the performances of ultrathin semiconductor nanomembrane-based optoelectronic devices such as photodetectors, solar cells, photocatalytic devices, luminescent devices.

Supporting Information Additional supporting information may be found in the online version of this article at the publisher's web-site.

Acknowledgements G. J. Li and Q. L. Guo contributed equally to this work. This work is supported by National Natural Science Foundation of China (Nos. 51322201, 51602056, and U1632115), China Postdoctoral Science Foundation (No. 2015M581523), Science and Technology Commission of Shanghai Municipality (No.14JC1400200), Open Project of State Key Lab of Silicon Materials (SKL2014-7), National Key Technologies R&D Program of China (2015ZX02102-003), and Changjiang Young Scholars Programme of China. Part of the experimental work has been carried out in Fudan Nanofabrication Laboratory.

References

[1] M. G. Lagally, MRS Bull. **32**, 57 (2007).
[2] J. A. Rogers, M. G. Lagally, and R. G. Nuzzo, Nature **477**, 45 (2011).
[3] G. Huang and Y. Mei, Adv. Mater. **24**, 2517 (2012).
[4] Q. Guo, M. Zhang, Z. Xue, G. Wang, D. Chen, R. Cao, G. Huang, Y. Mei, Z. Di, and X. Wang, Small **11**, 4140 (2015).
[5] O. Boyraz and B. Jalali, Opt. Express **12**, 5269 (2004).
[6] H. Yang, D. Zhao, S. Chuwongin, J.-H. Seo, W. Yang, Y. Shuai, J. Berggren, M. Hammar, Z. Ma, and W. Zhou, Nat. Photonics **6**, 617 (2012).
[7] K. R. Catchpole and S. Pillai, J. Lumin. **121**, 315 (2006).
[8] J. Yoon, A. J. Baca, S.-I. Park, P. Elvikis, J. B. Geddes, III., L. Li, R. H. Kim, J. Xiao, S. Wang, T.-H. Kim, M. J. Motala, B. Y. Ahn, E. B. Duoss, J. A. Lewis, R. G. Nuzzo, P. M. Ferreira, Y. Huang, A. Rockett, and J. A. Rogers, Nat. Mater. **7**, 907 (2008).
[9] B. Li, G. Li, E. Liu, Z. Jiang, J. Qin, and X. Wang, Appl. Phys. Lett. **73**, 3504 (1998).
[10] J.-H. Seo, K. Zhang, M. Kim, D. Zhao, H. Yang, W. Zhou, and Z. Ma, Adv. Opt. Mater. **4**, 120 (2016).
[11] J. Chu, Z. Han, F. Meng, and Z. Wang, Solid State Electron. **55**, 54 (2011).
[12] L. Menon, H. Yang, S. J. Cho, S. Mikael, Z. Ma, C. R. Hedlund, M. Hammar, and W. Zhou, IEEE Photonics J. **8**, 1 (2016).
[13] J. Sukmanowski, C. Paulick, O. Sohr, K. Andert, and F. X. Royer, J. Appl. Phys. **88**, 2484 (2000).
[14] B. Wang, T. Gao, and P. W. Leu, Nano Energy **19**, 471 (2015).
[15] B. Wang and P. W. Leu, Nano Energy **13**, 226 (2015).
[16] K. X. Wang, Z. Yu, V. Liu, Y. Cui, and S. Fan, Nano Lett. **12**, 1616 (2012).
[17] V. Sivakov, G. Andra, A. Gawlik, A. Berger, J. Plentz, F. Falk, and S. H. Christiansen, Nano Lett. **9**, 1549 (2009).
[18] S. Koynov, M. S. Brandt, and M. Stutzmann, Appl. Phys. Lett. **88**, 203107 (2006).
[19] J. Zhao, A. Wang, M. A. Green, and F. Ferrazza, Appl. Phys. Lett. **1991**, 73 (1998).
[20] C. M. Hsu, S. T. Connor, M. X. Tang, and Y. Cui, Appl. Phys. Lett. **93**, 133109 (2008).
[21] K. Qiu, Y. Zuo, T. Zhou, Z. Liu, J. Zheng, C. Li, and B. Cheng, J. Semicond. **36**, 10 (2015).
[22] D. Wang and G. Su, Sci. Rep. **4**, 7165 (2014).
[23] O. D. El, E. Drouard, G. Gomard, A. Kaminski, A. Fave, M. Lemiti, S. Ahn, S. Kim, P. C. I. Roca, H. Jeon, and C. Seassal, Opt. Express **18**, A293 (2010).
[24] Q. Guo, Y. Fang, M. Zhang, G. Huang, P. K. Chu, Y. Mei, Z. Di, and X. Wang, IEEE Trans. Electron Dev. **1985**, 64 (2017).
[25] G.-J. Lin, H.-P. Wang, D.-H. Lien, P.-H. Fu, H.-C. Chang, C.-H. Ho, C.-An. Lin, K.-Y. Lai, and J.-H. He, Nano Energy **6**, 36 (2014).
[26] T. Gao, E. Stevens, J.-K. Lee, and P. W. Leu, Opt. Lett. **39**, 4647 (2014).
[27] V. E. Ferry, L. A. Sweatlock, D. Pacifici, and H. A. Atwater, Nano Lett. **8**, 4391 (2008).
[28] J. Grandidier, D. M. Callahan, J. N. Munday, and H. A. Atwater, Adv. Mater. **23**, 1272 (2011).
[29] A. Raman, Z. Yu, and S. Fan, Opt. Express **19**, 19015 (2011).
[30] A. P. Vasudev, J. A. Schuller, and M. L. Brongersma, Opt. Express **20**, 385 (2012).
[31] T. Li, C. Zhou, and M. Jiang, Polym. Bull. **25**, 211 (1991).
[32] X. Hu, Y. Liu, B. Cheng, D. Zhang, and Q. Meng, Chin. Phys. Lett. **21**, 1289 (2004).
[33] M. L. Brongersma, Y. Cui, and S. Fan, Nat. Mater. **13**, 451 (2014).

[34] T. Maruyama and H. Minami, Sol. Energy Mater. Sol. Cells **79**, 113 (2003).
[35] P. Matheu, S. H. Lim, D. Derkacs, C. McPheeters, and E. T. Yu, Appl. Phys. Lett. **93**, 113108 (2008).
[36] T. Chang, P. Wu, S. Chen, C. Chan, C. Lee, C. Chen, and Y. Su, Opt. Express **17**, 6519 (2009).
[37] Y. H. Fu, A. I. Kuznetsov, A. E. Miroshnichenko, Y. Yu, and B. Lukyanchuk, Nature Commun. **4**, 1527 (2013).
[38] Z. Yang, P. Gao, C. Zhang, X. Li, and J. Ye, Sci. Rep. **6**, 30503 (2016).
[39] Y. Cao, K. Cai, P. Hu, L. Zhao, T. Yan, W. Luo, X. Zhang, X. Wu, K. Wang, and H. Zheng, Sci. Rep. **5**, 8130 (2015).
[40] H. M. Li, D. Y. Lee, S. C. Min, D. Qu, X. Liu, C. Ra, and W. Yoo, Sci. Rep. **4**, 447 (2014).
[41] E. D. Palik, Handbook of Optical Constants of Solids (Academic Press, New York, USA, 1985).
[42] N. Sultanova, S. Kasarova, and I. Nikolov, Acta Phy. Pol. A **116**, 585 (2009).
[43] D. Xiong, Z. Xu, X. Zeng, W. Zhang, Wei. Chen, Xiao. Xu, M. Wang, and Y. Cheng, J. Mater. Chem. A **22**, 24760 (2012).

